HHS Public Access

Author manuscript

Matrix Biol. Author manuscript; available in PMC 2017 October 22.

Published in final edited form as:

Matrix Biol. 2016 ; 52-54: 113–126. doi:10.1016/j.matbio.2016.02.007.

The Ameloblastin extracellular matrix molecule enhances bone fracture resistance and promotes rapid bone fracture healing

Xuanyu Lu[1,2], **Wenjin Li**[3], **Satoshi Fukumoto**[4], **Yoshihiko Yamada**[4], **Carla Evans**[2], **Thomas G.H. Diekwisch**[1,5], and **Xianghong Luan**[1,2]

[1]University of Illinois College of Dentistry, Brodie Laboratory for Craniofacial Genetics, Department of Oral Biology

[2]University of Illinois College of Dentistry, Brodie Laboratory for Craniofacial Genetics, Department of Orthodontics

[3]Department of Prosthodontics, University of Shanxi, Shanxi, China

[4]Craniofacial Developmental Biology and Regeneration Branch, National Institute of Dental and Craniofacial Research, National Institutes of Health, Bethesda, MD 20892, United States

[5]Texas A&M Baylor College of Dentistry, Department of Periodontics

Abstract

The extracellular matrix (ECM) provides structural support, cell migration anchorage, cell differentiation cues, and fine-tuned cell proliferation signals during all stages of bone fracture healing, including cartilaginous callus formation, callus remodeling, and bony bridging of the fracture gap. In the present study we have defined the role of the extracellular matrix protein ameloblastin (AMBN) in fracture resistance and fracture healing of mouse long bones. To this end, long bones from WT and AMBN$^{\Delta 5\text{-}6}$ truncation model mice were subjected to biomechanical analysis, fracture healing assays, and stem cell colony formation comparisons. The effect of exogenous AMBN addition to fracture sites was also determined. Our data indicate that lack of a functional AMBN in the bone matrix resulted in 31% decreased femur bone mass and 40% reduced energy to failure. On a cellular level, AMBN function inhibition diminished the proliferative capacity of fracture repair callus cells, as evidenced by a 58% reduction in PCNA and a 40% reduction in Cyclin D1 gene expression, as well as PCNA immunohistochemistry. In terms of fracture healing, AMBN truncation was associated with an enhanced and prolonged chondrogenic phase, resulting in delayed mineralized tissue gene expression and delayed ossification of the fracture repair callus. Underscoring a role of AMBN in fracture healing, there was a 6.9-fold increase in AMBN expression at the fracture site one week after fracture, and distinct AMBN immunolabeling in the fracture gap. Finally, application of exogenous AMBN protein to bone fracture sites accelerated callus formation and bone fracture healing (33% increase

Address for Correspondence: Xianghong Luan, MD, MS; or Tom Diekwisch, DMD, Ph.D., Ph.D., University of Illinois College of Dentistry, Brodie Laboratory for Craniofacial Genetics, Department of Oral Biology, 801 South Paulina, Chicago, IL, 60612, Phone: (312) 413 3545; luan@uic.edu or diekwisch@bcd.tamhsc.edu.

in bone volume and 19% increase in bone mineral density), validating the findings of our AMBN loss of function studies. Together, these data demonstrate the functional importance of the AMBN extracellular matrix protein in bone fracture prevention and rapid fracture healing.

INTRODUCTION

The extracellular matrix (ECM) of bone is a dynamic meshwork of self-assembled macromolecules that exerts profound control over all aspects of bone cell fate and behavior, including cell proliferation, survival, shape, migration and differentiation (1-4). The principal component of the bone ECM is type I collagen; however, the bone matrix is also rich in other non-collagenous structural proteins (e.g. fibronectin, laminin, and elastin), small integrin-binding proteins (SIBLING proteins, bone sialoprotein BSP, dentin matrix protein DMP1, matrix extracellular phosphoglycoprotein MEPE, and osteopontin OPN), matricellular proteins (e.g. tenascin-C, thrombospondin, SPARC), proteoglycans (asporin, biglycan, decorin, keratocan), enzymes (e.g. metalloproteinases), and growth factors (e.g. insulin growth factors IGF, transforming growth factors TGF, and bone morphogenetic proteins BMP). This complex macromolecular network not only provides strength and connectivity to the mineralized apatite nanoskeleton of bone, but also allows for a dynamic and highly specific response to traumatic stimuli, including injury and fracture.

Ameloblastin (AMBN) is one such extracellular matrix protein that contributes to the many functions of the mineralized tissue matrix (5). Originally discovered as the second most prominent enamel matrix protein (6, 7), AMBN has since been detected in many other tissues including dentin, cementum, pulp, and cranial bones (8). Explaining its multiple functions in development and regeneration, AMBN is related to the osteonectin (SPARC) ancestor SPARCL1, together with other enamel proteins including amelogenin and enamelin (9). As a bone extracellular matrix protein, AMBN affects Msx signaling (10, 11), integrin signaling (12), and cell adhesion through RhoA signaling (13).

The protein phase of the bone extracellular matrix plays important roles not only in bone development and maintenance, but also in response to bone injury and fracture. Bone fractures repairs are among the most commonly performed orthopedic procedures in the United States, with an approximate number of 7 million visits per year (14). While the majority of fractures respond to therapy and regain their original structure and function in a scarless manner, occasionally fracture healing may be delayed or result in a non-union outcome (15). Delayed or failed fracture repair increases the cost of care, necessitates additional surgeries, and results in a prolonged period of convalescence, associated with increased mortality in an aged population (16). Common therapeutic strategies for secondary fracture repair such as autologous bone grafts and bone morphogenetic protein applications have well-documented limitations (17). The high prevalence of bone fractures and the potential for failed fracture repair in osteoporotic and diabetic patients calls for novel approaches and reagents to improve bone fracture healing.

In the present study we have turned to the extracellular matrix protein AMBN as a bone matrix candidate molecule involved in the resistance of the physiological bone matrix against bone fracture and a potential new matrix component that may help to promote

fracture healing and repair. Based on our studies related to AMBN in calvarial growth, we have speculated that loss of full length AMBN may affect bone fracture resistance and repair. To test our hypothesis, we have applied a 3-point-bending test to determine the biomechanical properties of femurs from AMBN mutant littermates. Unilaterally open transverse tibial fractures were created to determine the effect of AMBN truncation on the molecular cascades and cellular processes that occur during fracture healing. AMBN deficient bone marrow stem cell populations were harvested to determine the role of AMBN in defining stem cell proliferation and differentiation capacity. And finally, to verify the role of AMBN in fracture healing, exogenous recombinant AMBN was applied to fracture sites as a means to evaluate its effect on new bone growth and fracture gap integrity. Together, the studies described here will provide novel insights in the role of the AMBN extracellular matrix molecular in fracture prevention and repair.

RESULTS

Decreased femur bone mass and fracture resistance in AMBN$^{\Delta 5\text{-}6}$ mutant mice

Our previous studies have demonstrated that AMBN affects long bone development (19). To verify the presence of AMBN in the periosteal callus, immunohistochemistry was performed on long bone tissues seven days (D7) after bone fracture surgery. Immunoreactions demonstrated distinct AMBN localization in hypertrophic chondrocytes, mesenchymal cells, and osteoblasts (Fig. 1A). According to our real-time RT-PCR data, *Ambn* gene expression was 6.9-fold upregulated on D7, 3.4-fold increased on D14, 1.5-fold increased on D21, and then gradually decreased to control levels on D28 (Fig. 1C). The increase in AMBN levels on D7 and D14 was highly significant ($p<0.0001$)(Fig. 1C). Bone structure and mineral density are common predictors of fracture susceptibility in bones. Here we conducted a microCT analysis to assess the microanatomical parameters that might predispose AMBN$^{\Delta 5\text{-}6}$ mutated mice toward bone fractures. MicroCT images revealed a 31% reduction in trabecular bone mass and 13 % reduction in cortical bone thickness in AMBN homozygous mutant mice compared to WT controls (Fig. 1A). To assess the effect of AMBN mutation on long bone mechanical properties, femur biomechanical properties were tested using 3-point-bending studies. Compared to 3-month-old WT mice, the AMBN$^{\Delta 5\text{-}6}$ mutants exhibited a smaller midshaft total area but without statistical significance (Table 2; Fig. 1B). However, femur stiffness was 14% lower in homozygous mutant mice ($p<0.05$) (Table 2; Fig. 1B). In addition, the maximum force yield to failure in AMBN$^{\Delta 5\text{-}6}$ mice was decreased by 16% ($p<0.05$), the maximum stress was reduced by 10% ($p<0.05$), and the energy to failure decreased by 40% ($p<0.05$) when compared with WT littermates (Table 2; Fig. 1B).

Enlarged cartilaginous callus formation and delayed bone fracture healing in AMBN$^{\Delta 5\text{-}6}$ mice

To determine whether AMBN mutation-related bone defects affect bone fracture healing, AMBN mutant mice and WT controls were subjected to our lower leg fracture regimen. Following bone fracture, tibia from all experimental groups displayed a similar fracture pattern on radiographs, with a consistent transverse gap in the center of the tibia diaphysis (Fig. 2A). After one week (D7 post-operatively), the fracture gap remained open without any

indication of bony bridge formation, both in WT and AMBN$^{\Delta 5\text{-}6}$ mutant mice. On D21, the fracture space had turned increasingly radio-opaque, and on D28 of this study the gap was almost closed and filled with radiodense bone mineral (Fig. 2A).

Micro-CT data revealed an unbridged large callus in 3D images of the control mouse fracture on D7. On days 14 and 21 after surgery, the fracture displayed a partial (D14) and almost complete (D21) bony bridge between neighboring fracture ends (Fig. 2B). At this stage, the bony bridge was distinguished by a porous surface structure. On D28, the bony callus was completely integrated with the adjacent tibia ends in control mice (Fig.2B). In contrast, the D7 AMBN$^{\Delta 5\text{-}6}$ fracture callus was less advanced than the D7 control callus, and the bony bridge of the fracture gap remained incomplete on D14 (Fig.2B). From D21 to D28, the fracture gap in AMBN$^{\Delta 5\text{-}6}$ animals was bridged, but contained extensive perforated areas, which were not detected in wild type control animals. The callus bone volume/total volume (BV/TV) ratio at fracture sites was significantly decreased in AMBN$^{\Delta 5\text{-}6}$ mice compared to WT controls at all time points ($p<0.05$) (Fig. 2C). Callus bone mineral density values (BMD) in AMBN$^{\Delta 5\text{-}6}$ animals were decreased on days D7 and D14, but almost matched those of the wild type control on days D21 and D28 (Fig.2D).

The cartilaginous callus indicative of fracture healing was visualized on paraffin sections stained with Safranin O as a cartilage marker (Fig. 3A). On D7, the control group displayed a cartilaginous callus with periosteal ossification starting adjacent to the cartilage borders. On D14 in controls, the size of periosteal callus was comparable to that of AMBN mutant mice, however, the cartilaginous area was decreased, and ossification centers were detected on both sides of the cortical bone. On D21 and D28, the control callus was fully bridged with bone, and the cartilage was almost undetectable by Safranin O staining. At this stage, the cortical bone was largely remodeled. Compared to the fracture repair process in controls, cartilaginous callus formation in AMBN$^{\Delta 5\text{-}6}$ mice was distinctly different (Fig. 3A): The cartilaginous area in the callus on D7 and D14 was much larger in AMBN mutant mice than in controls, indicative of cartilage accumulation and of an unbridged bone fracture. By D21 and D28 in the AMBN mutant mice, the cartilage was almost undetectable and the fracture gap was closed, however, cortical bone continuity at the fracture site remained interrupted. The hard callus remained larger for a longer period of time compared to the callus in WT mice, indicating that remodeling was delayed. Histomorphometric analysis demonstrated a significant increase in the cartilage area/periosteal callus area (Cg.Ar./Ps.Cl.Ar.%) of D7 and D14 mice, while the mineralized area/periosteal callus area (Md.Ar./Ps.Cl.Ar.%) was reduced at all time points post-operatively ($p<0.05$) in AMBN$^{\Delta 5\text{-}6}$ mutant mice compared to wild type controls. By D28, Safranin O-labeled cartilage regions in both WT and AMBN mutant animals were almost undetectable.

Reduced cell proliferation, delayed mineralization gene expression, and enhanced chondrogenesis during fracture healing in AMBN$^{\Delta 5\text{-}6}$ mice

Through their control of proliferation and gene expression, extracellular matrix proteins such as AMBN exert profound control over cell number and fate during regeneration and repair. Here we have tested the effect of AMBN mutation on cell proliferation and key marker genes involved in endochondral ossification and bone remodeling, including bone markers

Runx2, *osteopontin*, *osteocalcin*, and *collagen I*, as well as cartilage markers *Sox9* and *collagen II*. The effect of AMBN on proliferation was assessed using PCNA cell counting morphometry as well as cyclin D1 and PCNA gene expression analysis.

Morphometric evaluation of PCNA protein expression and localization data revealed a significant decrease in the number of PCNA+ cells among undifferentiated mesenchymal cells (49%), pre-hypertrophic chondrocytes (54%) and immature bone cells (55%) in AMBN$^{\Delta 5\text{-}6}$ mice compared with WT mice (Fig. 4A, B). The decrease in the number of PCNA+ proliferative cells was correlated with the changes in the gene expression of proliferation markers PCNA and Cyclin D1 at same stages of fracture healing in AMBN$^{\Delta 5\text{-}6}$ mice. Both cyclin D1 and PCNA gene expression were downregulated on post-fracture days D7, D14 and D21, with a significant reduction of cyclin D1 on days on D14 (40%) and D21 (20%), and a more than 50% significant reduction in PCNA levels on D7 (58%) and D14 (55%) (Fig. 4C). Together, these data indicate that cell proliferation rates at the fracture repair site in the AMBN mutant group were approximately half of those of the control group.

To further understand the mechanism of delayed fracture healing, expression of osteoblastic and chondrogenic marker genes were determined by qRT-PCR. Our data indicate that *Runx2*, *Ocn, Opn* and *Col1a1* levels were significantly reduced by days 7 and 14 in AMBN mutants compared to WT mice. The downregulation of these genes was reversed on D21 (Fig. 4), indicating a delayed onset of mineralization gene expression in AMBN mutant mice. In contrast, *Sox9* and *Col 2a1* gene expression in AMBN$^{\Delta 5\text{-}6}$ mice was enhanced at all time points, reflective of the increased levels of chondrogenesis observed during tibia fracture healing in mice expressing a truncated AMBN (Fig. 4C).

Reduced proliferation and differentiation potential in bone marrow stromal stem cells generated from AMBN$^{\Delta 5\text{-}6}$ mice

To ask whether the reduction in proliferation and differentiation potential in AMBN mutant mice is a property of AMBN mutant stem cells or a secondary feature acquired at later stages of development, we compared stemness characteristics, proliferation and differentiation capacity of AMBN mutant BMSCs to WT BMSCs using colony forming unit (CFU) assays. These assays revealed that CFU-fibroblast numbers (CFU-F), and CFU-osteoblast numbers (CFU-Ob) were significantly reduced in AMBN$^{\Delta 5\text{-}6}$ mice when compared with WT and AMBN^{HET} mutant controls ($p<0.05$) (Figs.5 A, C, D). The size of CFU-F colonies and the number of cells within the colony were also significantly reduced in cells cultured from AMBN mutant mice (Fig.5 A). In addition, the area occupied by mineralized matrix as revealed by alizarin red staining was smaller in AMBN homozygous mutant cell populations when compared to controls (Fig. 5C). Following 18 days of chondrogenic induction, culture aggregates were positive for Safranin O and Alcian blue staining in WT mice. In contrast, Safranin O and Alcian blue staining was almost absent in AMBN$^{\Delta 5\text{-}6}$ mice (Fig. 5B). This finding indicates that the number of mesenchymal stem cells in the bone marrow of AMBN$^{\Delta 5\text{-}6}$ mice was reduced, and their cell proliferation and differentiation potential was diminished.

Accelerated bone fracture healing following application of exogenous AMBN protein

Data presented so far indicated that AMBN mutation resulted in delayed tibia fracture healing. We thus asked whether application of exogenous AMBN protein was a suitable strategy to accelerate bone fracture healing. To address this question, AMBN- or PBS-coated collagen sponges were surgically implanted at the tibia fracture sites for 7, 14 and 21 days. X-ray images demonstrated a similar fracture pattern between PBS control and AMBN treatment groups (Supplement Fig.1). MicroCT analysis revealed that exogenous application of AMBN protein via collagen sponge delivery increased bone volume at the fracture zone by 33% on D21 (Fig. 6A, B). There was also an increase in bone mineral density values by 19% on D21 following exogenous AMBN application (Fig. 6A, B). While there was an increase in bone parameters including bone volume and mineral density on post-surgery days D14 and D21, AMBN application promoted chondrogenesis and ossification at the earlier D7 time point of fracture healing as revealed by H&E staining of a fracture representative mid-section through the fracture (Fig. 6C). This micrograph demonstrates a cartilaginous callus in the AMBN treated group while the control fracture was occupied by granulation tissue, containing mesenchymal cells, chondrocytes and fibroblasts (Fig. 6C). The AMBN induced rapid shift in the chrondrogenesis/osteogenesis balance during fracture healing was matched by a corresponding increase in BMP7 (64%), Sox9 (66%) and Collagen 2a1 (72%) on D7. Collagen I expression was almost twice as high in the AMBN treatment group on D14 when compared to the control. However, both BMP7 and Collagen I continuously increased in the in PBS-treated control group until D21, when they exceeded AMBN treatment group levels by 41% (BMP7) and 358% (Col1) (Fig. 6D), indicating that AMBN promoted rapid osteogenic and chondrogenic gene expression at an early stage of fracture healing.

DISCUSSION

In the present study we used a tibia bone fracture model to assess the function of the ameloblastin extracellular matrix molecule as an integral component of the bone matrix as it relates to physiological fracture resistance and fracture healing, and as a potential therapeutic agent to accelerate fracture repair and regeneration. Our data indicate that lack of a functional AMBN in the bone matrix resulted in decreased femur bone mass and fracture resistance. On a cellular level, AMBN function inhibition diminished the proliferative capacity of bone marrow stromal cells, chondrocytes, and osteoblasts within the fracture repair callus. In terms of fracture healing, AMBN truncation was associated with an enhanced and prolonged chondrogenic phase, resulting in delayed mineralized tissue gene expression and delayed ossification of the fracture repair callus. Finally, application of exogenous AMBN protein to bone fracture sites accelerated callus formation and bone fracture healing, validating the findings of our AMBN loss of function studies. Together, these studies demonstrate the functional importance of the AMBN extracellular matrix protein in the prevention of bone fracture and for the promotion of rapid fracture healing.

Our study demonstrated that lack of a functional AMBN in the bone matrix resulted in decreased femur bone mass and fracture resistance. Bone strength, stiffness, and fracture resistance depend on its mineral phase and on its surrounding extracellular matrix (19-31).

Changes in ECM composition as implemented here through AMBN loss of function affect bone quality through a number of mechanisms, including effects on the remodeling of the structural aspects of the extracellular matrix including collagen and collagen cross-links, effects on the physical properties of the ECM (e.g. bound water content), altered growth factor signaling such as TGF-β signaling, and changes in transcriptional regulation through Runx2 and other transcription factors (22, 25). The bone ECM is also directly responsible for bone mineralization and bone mineral content (26, 27) and calcium binding proteins such as AMBN (5) are likely to affect mineral nucleation and mineral binding to the bone extracellular matrix. In addition, the bone ECM contributes to a non-fibrous organic matrix that facilitates bone strength and fracture resistance by interconnecting mineralized collagen fibrils (28) and AMBN with its adhesion domains and attachment induction properties is likely instrumental in gene expression regulation through the RhoA pathway (18, 29). Together, this evidence suggests that loss of AMBN affects femur bone mass and femur fracture resistance by disrupting the finely woven multidimensional meshwork of bone ECM molecule, which in turn alters mineralized tissue homeostasis and mechanical properties.

On a cellular level, AMBN function inhibition diminished the proliferative capacity of chondrocytes, and osteoblasts within the fracture repair callus and also among bone marrow stromal stem cells generated from $AMBN^{\Delta 5\text{-}6}$ mice. In our study, the negative effect of AMBN loss of function on proliferation when compared to wild-type controls was verified on three different levels, (i) by proliferating nuclear antigen (PCNA) immunohistochemistry of undifferentiated mesenchymal cells, pre-hypertrophic chondrocytes, and immature osteoblast and osteocytes on paraffin sections, (ii) by real-time RT-PCR comparison of cyclin D1 and PCNA expression levels one, two, and three weeks after fracture, and (iii) by assessing the number of colony-forming units (CFUs) from BMSCs. The effect of extracellular matrix proteins on the ability of cells to either proliferate or exit the cell cycle depends on a variety of factors, including the cell type, the type of matrix protein or factor, the concentration of the protein or factor, and on the level of cell attachment to surfaces. The present study appears to indicate that BMSCs and most cell types within the fracture callus require functional AMBN to reach their full proliferative potential, and this may be related to AMBN's role in adhesion and matrix organization. The role of AMBN in fracture healing is further underscored by the increase of AMBN expression during fracture healing and the high levels of AMBN protein in the fracture gap. However, there is no general consensus in the recent literature whether the effect of AMBN on cell cycle progression is of stimulatory or repressive nature. Some studies (30, 31) conclude that AMBN promotes bone growth, while others (10, 11, 13) report a repressive effect of ameloblastin in calvarial sutures and periodontal ligament fibroblasts. As discussed earlier (13), seemingly contradictory effects are likely due to different AMBN functions in various cell types or the result of interactions between multiple AMBN domains with various matrix proteins or cell surface receptors, or the dose-dependency of AMBN expression caused by either overexpression or knockout of the *Ambn* gene (32, 33). Such diversity in function is exerted by many extracellular matrix proteins, including AMBN's close relative osteonectin (SPARC) that is known to either inhibit or promote proliferation/growth, depending on cell type and environment (34).

In terms of fracture healing, AMBN truncation was associated with an accumulation of cartilage and a prolonged chondrogenic phase, resulting in a delay in mineralized tissue gene

expression and delayed ossification of the fracture repair callus. In this respect, AMBN joins a long list of extracellular matrix molecules, transcription and growth factors that have been associated with delayed fracture healing in knockout mouse models, including β-catenin, FGF9, PTH, MMP2, OPN, and BSP (35, 36). The great number of factors involved in delayed or accelerated fracture healing is indicative of the plethora of molecules that are involved in the multifactorial process of fracture gap bridging and replacement with functional bone. However, our data not only demonstrate the importance of functional AMBN for timely and physiological fracture healing in mice, they also provide new insights into the biological process of fracture callus transformation into functional bone, as they imply that the mineralization protein AMBN might be responsible for the rapid tipping of the chondrogenesis/osteogenesis balance toward an osteogenic phenotype (37, 38). AMBN might have three functions in this process, (i) to provide additional templating sites for bone mineralization, (ii) to enhance cell adhesion as a requirement for mineralized tissue formation, and (iii) to modulate osteogenic signaling via BMPs, Runx2 and Osx. Differences between our findings indicating that loss of AMBN function results in delayed bone fracture healing and a previous report (39) are likely due to differences in data interpretation and analysis techniques.

Perhaps the most exciting aspect of our study was the accelerated callus formation and bone fracture healing following application of exogenous AMBN protein to a bone fracture site. This study was originally conducted as a proof-of-principle to verify the findings from our AMBN loss of function studies. As it turned out, AMBN appeared to both promote initial cartilaginous callus formation and subsequent transformation into a faithful bony bridge between fracture ends. Even though the 20% increase in bone volume reported in our current study was somewhat modest, it was significant and might be of great therapeutic benefit especially in osteoporotic or diabetic patients. Moreover, our discovery of AMBN-mediated accelerated bone fracture healing might be further enhanced using different formulations or delivery systems. This finding is the first report of a potential therapeutic use of exogenous AMBN for future clinical fracture healing applications. The role of AMBN in bone fracture healing begs comparison with a commercially available product, Emdogain (EMD), an enamel matrix derivative that lists AMBN and another enamel protein, amelogenin (AMEL), among its components. Literature reviews report varying results of EMD on bone formation and find that the regenerative response of EMD in periodontal tissues is only partly replicated by amelogenin or ameloblastin components (40), while our studies clearly support the concept of AMBN as a beneficial molecule during long bone fracture healing.

EXPERIMENTAL PROCEDURES

Experimental animals

Studies are based on an AMBN loss of function mouse model generated by disrupting expression of full-length AMBN by deletion of exons 5 and 6 ($AMBN^{\Delta 5\text{-}6}$) (10). For the present study, AMBN mutated mice were backcrossed with C57BL/6 mice for 10 generations to create genomic homogenized heterozygous breeders. The AMBN wild-type (WT), heterozygous mutant ($AMBN^{HET}$) and homozygous mutant ($AMBN^{\Delta 5\text{-}6}$) were generated using a 1 male and 2 female mating approach for heterozygote-heterozygote

crossing. Genotyping was performed by PCR analysis of genomic DNA extracted from mouse tail clips, using R1 primers to detect the wild type allele and a neomycin primer (R2) to detect the targeted allele (Table 1). All experimental protocols and animal handling were approved by Committee on the Ethics of Animal Experiments of the University of Illinois at Chicago.

X-ray and micro-CT analysis

X-ray radiographic analysis was performed on fracture samples in both antero-posterior and lateral directions immediately post fracture to ensure faithful representation of fracture pattern and fixation needle position. The fracture healing properties were examined on days 7 (D7), 14 (D14), 21 (D21) and 28 (D28) post-surgery with 30.0 kV for a duration of 10.0 s (n=5-6, Faxitron X-ray, Wheeling, IL). Micro-CT analysis was performed using a 10.5 μm isotropic resolution (n=5, Scanco viva CT 40, Scanco Medical AG, Switzerland) to examine the entire length of the callus at each time point. Callus mineralized volume fraction (BV/TV) (%) and connectivity density (Conn.D, $1/mm^3$) were calculated to describe bone tissue structure and porosity (41).

Biomechanical testing

Femurs from 3 months old male WT and AMBN mutant littermates (n=5 per group) were used for 3-point femur bending tests as previously described (42, 43). To collect a sufficient number of samples for subsequent biomechanical analysis, femurs were isolated immediately after sacrifice of WT and AMBN mutant mice. Following isolation, femur samples were fixed in 70% ethanol and frozen in -20°C for later use. On the day of testing, the femurs were thawed and rehydrated with 1×PBS for 3 hours. Three-point bending was performed with a support span of 6.0 mm. Femurs were loaded at the midshaft perpendicularly to the long axis of the bone and with the load applied in the anterior to posterior direction. Samples were tested to failure at a deflection rate of 5 mm/min using a custom anvil (42). Bending force-deflection curves were constructed and analyzed for stiffness (N/mm) and maximum force to failure (N). The energy to failure (N*mm) was calculated from the classical equations of beam theory for a simple supported beam with a central concentrated load (42, 43).

Fracture model

The surgery procedure was approved by the Animal Ethics Committee of the University of Illinois at Chicago and carried out according to the Guidelines for the Care and Use of Laboratory Animals. A unilateral left side open transverse tibia fracture with intramedullary needle fixation (44) was employed as the bone fracture model in the present study. Three-month old WT and $AMBN^{\Delta 5\text{-}6}$ male mice (6 mice per group) were anesthetized with ketamine (100mg/kg) and Xylazine (5 mg/kg) by intraperitoneal injection. Buprenorphine (0.01 mg/kg) was administrated subcutaneously once prior to surgery and three times a day during the first 3 days after surgery to relieve pain. A 1.5 cm long skin incision was made along the anterior-medial surface of the tibia. At the medial side of the patellar ligament, a 27 gauge syringe needle was inserted into the bone marrow cavity of the tibia through the tibial plateau, to establish a pin canal and enlarge the marrow cavity. The needle was then removed, and a No.11 surgical blade was used to transect the diaphysis of the tibia at the

middle point of the diaphysis shaft, followed by inserting a 25 gauge syringe needle. The periosteum was kept intact. To protect the soft tissues and the surgical site, the wound was closed using sutures.

AMBN rescue studies

For exogenous AMBN protein application, collagen sponges were coated with AMBN full length protein (10 μg/ml) at 4°C overnight and then lyophilized. PBS served as a control for the collagen sponge coating. Tibia fractures were generation as described above using 3 months old WT C57BL/6 mice (6 mice per group). The AMBN- or PBS-coated collagen sponges were placed at the fracture site between tibia and Tibialis anterior. The effect of exogenous AMBN protein on fracture healing was examined on days D7, D14 and D21 post-surgery.

Skeletal preparation

The tibia samples were dissected from the femurs, ankles and overlying skin of the surgical side post-operatively on postnatal days 7, 14, 21 and 28. During the dissection, callus tissue was carefully protected by retaining sufficient muscle, and the intramedullary needle was removed. Harvested samples were prepared for X-ray, micro-CT, histology and mRNA isolation.

Histology and Histomorphometry

Bone samples were serially fixed in 10% normal buffered formalin overnight, decalcified and embedded in paraffin. Tissue sections at the fracture site were cut longitudinally and prepared for H&E staining, Safarin O/fast green staining, and immunohistochemistry. For Safarin O/fast green staining, the paraffin sections were stained with hematoxylin working solution after deparaffinization and rehydration, stained with 0.05% fast green solution, quickly rinsed with 1% acetic acid and stained in 0.1% safranin O solution. Histomorphometric analysis (n=5 at each time point) was conducted using Image-Pro Plus 4.5 software (Media Cybernetics, Cambridge, UK). The diameter of the tibia was used a baseline to define the size of the region of interest (ROI) (Fig. 3B). The callus was divided into a proximal and a distal part, and a 1.5 length of the baseline was used to define the proximal and distal callus halves of the ROI. The total diameter of the callus was included in the ROI. The mineralized volume of the cortices, the area of the periosteal calluses, and the mineralized and cartilaginous volume of the calluses were measured and compared between groups (45, 46). The structural indices were calculated as mineralized area of the corticalis (Ct): Mineralized area/Cortical Bone area (Md.Ar/Ct.B.Ar) (%) and cartilage area of the periosteal callus area: Cartilage area/Periosteal callus area (Cg.Ar/Ps.Cl.Ar) (%). For immunostaining, sections prepared from bone samples 7 days after fracture surgery were incubated with Rabbit anti-Proliferating Cell Nuclear Antigen (PCNA) antibody (Abcam, Cambridge, MA) or affinity purified AMBN antibody (18) at 4 °C overnight, and then with anti-rabbit secondary antibody (Abcam). Protein expression was detected with a Histomouse Broad Spectrum AEC (Invitrogen, Carlsbad, CA). Images were acquired in areas of undifferentiated mesenchymal, pre-hypertrophic chondrocytes and immature bone for morphometric analysis of percent PCNA positive cells at each stage of fracture healing.

Quantitative gene expression analysis

The callus of the fracture site with 1 mm of adjacent bone tissue on both proximal and distal sides was harvested and total RNA was extracted using the Qiagen RNeasy Minikit (n=5 in each time point). The iScript cDNA Synthesis Kit (Bio-Rad, Hercules, CA) was used to synthesize cDNA from 1 μg of RNA per callus. Real-time PCR analysis was performed with mouse specific primers for chondrocyte and osteoblast marker genes (Table 1). The relative expression level was computed using the $2^{-\Delta\Delta Ct}$ analysis method, and actin was used as an internal reference (47).

Bone marrow stromal cell (BMSC) isolation and characterization

BMSCs were flushed from femurs and tibiae of 3 months old WT, $AMBN^{HET}$ and $AMBN^{\Delta 5\text{-}6}$ littermates. The cell suspensions were filtered through a 40 μm cell strainer (Becton-Dickinson, Franklin Lakes, NJ) to obtain single cells. Nucleated cells were plated in 35 mm dishes at a density of 0.5×10^5/well in complete MesenCult medium (STEMCELL Technologies, Vancouver, Canada) with duplicated cultures. For the Colony Forming Unit-fibroblast numbers (CFU-F) assay, cell cultures were fixed and stained with Giemsa. For the CFU-osteoblast numbers (CFU-Ob) assay, BMSCs were cultured in growth medium for 14 days, followed by osteogenic medium (Lonza) for 7 days, and then analyzed for mineralized matrix formation by alizarin red staining. We determined the colony-forming efficiency by quantifying the number of colonies per 10^5 marrow cells. For chondrogenesis in standard pellet culture, 2×10^5 BMSCs were pelleted by centrifugation and cultured in chondrogenic medium (Lonza) for 18 days. The cultured pellets were then processed for histochemical analysis as previously described (48).

Statistical analysis

Quantitative data were presented as means ± SD and compared with analysis of one way ANOVA. The difference between groups was considered statistically significant at $p< 0.05$.

Supplementary Material

Refer to Web version on PubMed Central for supplementary material.

Acknowledgments

Generous support by NIDCR grant R01 DE019155 to XL is gratefully acknowledged.

References

1. Giancotti FG, Ruoslahti E. Integrin signaling. Science. 1999; 285:1028–1032. [PubMed: 10446041]
2. Okazaki K, Sandell LJ. Extracellular matrix gene regulation. Clin Orthop Relat Res. 2004; 427(Suppl):S123–128.
3. Daley WP, Peters SB, Larsen M. Extracellular matrix dynamics in development and regenerative medicine. J Cell Sci. 2008; 121(Pt 3):255–264. [PubMed: 18216330]
4. Gentili C, Cancedda R. Cartilage and bone extracellular matrix. Curr Pharm Des. 2009; 15:1334–1348. [PubMed: 19355972]

5. Zhang X, Diekwisch TG, Luan X. Structure and function of ameloblastin as an extracellular matrix protein: adhesion, calcium binding, and CD63 interaction in human and mouse. Eur J Oral Sci. 2011; 119(Suppl 1):270–279. [PubMed: 22243256]
6. Krebsbach PH, Lee SK, Matsuki Y, Kozak CA, Yamada KM, Yamada Y. Full-length sequence, localization, and chromosomal mapping of ameloblastin. A novel tooth-specific gene. J Biol Chem. 1996; 271:4431–4435. [PubMed: 8626794]
7. Lu X, Ito Y, Kulkarni A, Gibson C, Luan X, Diekwisch TG. Ameloblastin-rich enamel matrix favors short and randomly oriented apatite crystals. Eur J Oral Sci. 2011; 119(Suppl 1):254–260. [PubMed: 22243254]
8. Atsawasuwan P, Lu X, Ito Y, Chen Y, Gopinathan G, Evans CA, Kulkarni AB, Gibson CW, Luan X, Diekwisch TG. Expression and function of enamel-related gene products in calvarial development. J Dent Res. 2013; 92:622–628. [PubMed: 23625374]
9. Sire JY, Delgado S, Fromentin D, Girondot M. Amelogenin: lessons from evolution. Arch Oral Biol. 2005; 50:205–212. [PubMed: 15721151]
10. Fukumoto S, Kiba T, Hall B, Iehara N, Nakamura T, Longenecker G, Krebsbach PH, Nanci A, Kulkarni AB, Yamada Y. Ameloblastin is a cell adhesion molecule required for maintaining the differentiation state of ameloblasts. J Cell Biol. 2004; 167:973–983. [PubMed: 15583034]
11. Atsawasuwan P, Lu X, Ito Y, Zhang Y, Evans CA, Luan X. Ameloblastin inhibits cranial suture closure by modulating MSX2 expression and proliferation. PLoS One. 2013; 8:e528.
12. Lu X, Ito Y, Atsawasuwan P, Dangaria S, Yan X, Wu T, Evans CA, Luan X. Ameloblastin modulates osteoclastogenesis through the integrin/ERK pathway. Bone. 2013; 54:157–168. [PubMed: 23385480]
13. Zhang Y, Zhang X, Lu X, Atsawasuwan P, Luan X. Ameloblastin regulates cell attachment and proliferation through RhoA and p27. Eur J Oral Sci. 2011; 119(Suppl 1):280–285. [PubMed: 22243257]
14. Praemer, A., Furner, S., Rice, DP. Musculoskeletal Conditions in the United States. 1. American Academy of Orthopaedic Surgeons; Rosemont, IL: 1999.
15. Gómez-Barrena E, Rosset P, Lozano D, Stanovici J, Ermthaller C, Gerbhard F. Bone fracture healing: Cell therapy in delayed unions and nonunions. Bone. 2015; 70:93–101. [PubMed: 25093266]
16. Streubel PN, Ricci WM, Wong A, Gardner MJ. Mortality after distal femur fractures in elderly patients. Clin Orthop Relat Res. 2011; 469:1188–1196. [PubMed: 20830542]
17. Oryan A, Alidadi S, Moshiri A. Current concerns regarding healing of bone defects. Hard Tissue. 2013; 2:13.
18. Lu X, Fukumoto S, Yamada Y, Evans CA, Diekwisch TG, Luan X. Ameloblastin, an Extracellular Matrix Protein, Affects Long Bone Growth and Mineralization. J Bone Miner Res. 2016; doi: 10.1002/jbmr.2788
19. Burstein AH, Zika JM, Heiple KG, Klein L. Contribution of collagen and mineral to the elastic-plastic properties of bone. J Bone Joint Surg Am. 1975; 57:956–961. [PubMed: 1184645]
20. Boskey AL. Matrix proteins and mineralization: an overview. Connect Tissue Res. 1996; 35:357–363. [PubMed: 9084675]
21. Kanis JA. Diagnosis of osteoporosis and assessment of fracture risk. Lancet. 2002; 359:1929–1936. [PubMed: 12057569]
22. Nyman JS, Makowski AJ. The contribution of the extracellular matrix to the fracture resistance of bone. Curr Osteoporos Rep. 2012; 10:169–177. [PubMed: 22527725]
23. Alford AI, Kozloff KM, Hankenson KD. Extracellular matrix networks in bone remodeling. Int J Biochem Cell Biol. 2015; 65:20–31. [PubMed: 25997875]
24. Eckes B, Zigrino P, Kessler D, Holtkötter O, Shephard P, Mauch C, Krieg T. Fibroblast-matrix interactions in wound healing and fibrosis. Matrix Biol. 2000; 19:325–332. [PubMed: 10963993]
25. Alliston T. Biological regulation of bone quality. Curr Osteoporos Rep. 2014; 12:366–375. [PubMed: 24894149]
26. Marsh ME, Munne AM, Vogel JJ, Cui Y, Franceschi RT. Mineralization of bone-like extracellular matrix in the absence of functional osteoblasts. J Bone Miner Res. 1995; 10:1635–1643. [PubMed: 8592939]

27. Murshed M, McKee MD. Molecular determinants of extracellular matrix mineralization in bone and blood vessels. Curr Opin Nephrol Hypertens. 2010; 19:359–365. [PubMed: 20489614]
28. Fantner GE, Hassenkam T, Kindt JH, Weaver JC, Birkedal H, Pechenik L, Cutroni JA, Cidade GA, Stucky GD, Morse DE, Hansma PK. Sacrificial bonds and hidden length dissipate energy as mineralized fibrils separate during bone fracture. Nat Mater. 2005; 4:612–16. [PubMed: 16025123]
29. Hatekeyama J, Fukumoto S, Nakamura T, Hauyama N, Suzuki S, Hatekeyama Y, Shum L, Gibson CW, Yamada Y, Kulkarni AB. Synergistic roles of amelogenin and ameloblastin. J Dent Res. 2009; 88:318–322. [PubMed: 19407150]
30. Zeichner-David M, Chen LS, Hsu Z, Reyna J, Caton J, Bringas P. Amelogenin and ameloblastin show growth-factor like activity in periodontal ligament cells. Eur J Oral Sci. 2006; 114(Suppl 1): 244–253. [PubMed: 16674693]
31. Tamburstuen MV, Reppe S, Spahr A, Sabetrasekh R, Kvalheim G, Slaby I, Syversen U, Lyngstadaas SP, Reseland JE. Ameloblastin promotes bone growth by enhancing proliferation of progenitor cells and by stimulating immunoregulators. Eur J Oral Sci. 2010; 118:451–459. [PubMed: 20831578]
32. Paine ML, Wang HJ, Luo W, Krebsbach PH, Snead ML. A transgenic animal model resembling amelogenesis imperfecta related to ameloblastin overexpression. J Biol Chem. 2003; 278:19447–19452. [PubMed: 12657627]
33. Chun YH, Lu Y, Hu Y, Krebsbach PH, Yamada Y, Hu JC, Simmer JP. Transgenic rescue of enamel phenotype in Ambn null mice. J Dent Res. 2010; 89:1414–1420. [PubMed: 20940352]
34. Sangaletti S, Tripodo C, Cappetti B, Casalini P, Chiodoni C, Piconese S, Santangelo A, Parenza M, Arioli I, Miotti S, Colombo MP. SPARC oppositely regulates inflammation and fibrosis in bleomycin-induced lung damage. Am J Pathol. 2011; 179:3000–3010. [PubMed: 22001347]
35. Huang Y, Zhang X, Du K, Yang F, Shi Y, Huang J, Tang T, Chen D, Dai K. Inhibition of β-catenin signaling in chondrocytes induces delayed fracture healing in mice. J Orthop Res. 2012; 30:304–310. [PubMed: 21818768]
36. Abou-Khalil R, Colnot C. Cellular and molecular bases of skeletal regeneration: what can we learn from genetic mouse models? Bone. 2014; 64:211–21. [PubMed: 24709685]
37. Wang M, Li S, Xie W, Shen J, Im HJ, Holz JD, Wang M, Diekwisch TG, Chen D. Activation of β-catenin signalling leads to temporomandibular joint defects. Eur Cell Mater. 2014; 28:223–235. [PubMed: 25340802]
38. Jing Y, Zhou X, Han X, Jing J, von der Mark K, Wang J, de Crombrugghe B, Hinton RJ, Feng JQ. Chondrocytes Directly Transform into Bone Cells in Mandibular Condyle Growth. J Dent Res. 2015; 94:1668–1675. [PubMed: 26341973]
39. Kuroda S, Wazen R, Sellin K, Tanaka E, Moffatt P, Nanci A. Ameloblastin is not implicated in bone remodelling and repair. Eur Cell Mater. 2011; 22:56–66. [PubMed: 21761392]
40. Grandin HM, Gemperli AC, Dard M. Enamel matrix derivative: a review of cellular effects in vitro and a model of molecular arrangement and functioning. Tissue Eng Part B Rev. 2012; 18:181–202. [PubMed: 22070552]
41. Kallai I, van Lenthe GH, Ruffoni D, Zilberman Y, Müller R, Pelled G, Gazit D. Quantitative, structural, and image-based mechanical analysis of nonunion fracture repaired by genetically engineered mesenchymal stem cells. J Biomech. 2010; 43:2315–2320. [PubMed: 20471652]
42. Ferguson VL, Ayers RA, Bateman TA, Simske SJ. Bone development and age-related bone loss in male C57BL/6J mice. Bone. 2003; 33:387–398. [PubMed: 13678781]
43. Margolis DS, Kim D, Szivek JA, Lai LW, Lien YH. Functionally improved bone in calbindin-D28k knockout mice. Bone. 2006; 39:477–484. [PubMed: 16631426]
44. Mi M, Jin H, Wang B, Yukata K, Sheu TJ, Ke QH, Tong P, Im HJ, Xiao G, Chen D. Chondrocyte BMP2 signaling plays an essential role in bone fracture healing. Gene. 2013; 512:211–218. [PubMed: 23107765]
45. Parfitt AM, Drezner MK, Glorieux FH, Kanis JA, Malluche H, Meunier PJ, Ott SM, Recker RR. Bone histomorphometry: standardization of nomenclature, symbols and units. J Bone Miner Res. 1987; 2:595–610. [PubMed: 3455637]

46. Schmidmaier G, Wildemann B, Heeger J, Gäbelein T, Flyvbjerg A, Bail HJ, Raschke M. Improvement of fracture healing by systemic administration of growth hormone and local application of insulin-like growth factor-1 and transforming growth factor-beta1. Bone. 2002; 31:165–172. [PubMed: 12110430]

47. Livak KJ, Schmittgen TD. Analysis of relative gene expression data using real-time quantitative PCR and the $2^{-\Delta\Delta Ct}$ Method. Methods. 2001; 25:402–408. [PubMed: 11846609]

48. Luan X, Ito Y, Dangaria S, Diekwisch TG. Dental follicle progenitor cell heterogeneity in the developing mouse periodontium. Stem Cells Dev. 2006; 15:595–608. [PubMed: 16978062]

Highlights

- Lack of a functional AMBN in the bone matrix resulted in 31% decreased femur bone mass and 40% reduced energy to failure.
- AMBN function inhibition diminished the proliferative capacity of fracture repair callus cells, as evidenced by a 58% reduction in PCNA and a 40% reduction in Cyclin D1 gene expression, as well as PCNA immunohistochemistry.
- AMBN truncation was associated with an enhanced and prolonged chondrogenic phase, resulting in delayed mineralized tissue gene expression and delayed ossification of the fracture repair callus.
- There was a 6.9-fold increase in AMBN expression at the fracture site one week after fracture, and distinct AMBN immunolabeling in the fracture gap.
- Application of exogenous AMBN protein to bone fracture sites accelerated callus formation and bone fracture healing (33% increase in bone volume and 19% increase in bone mineral density).

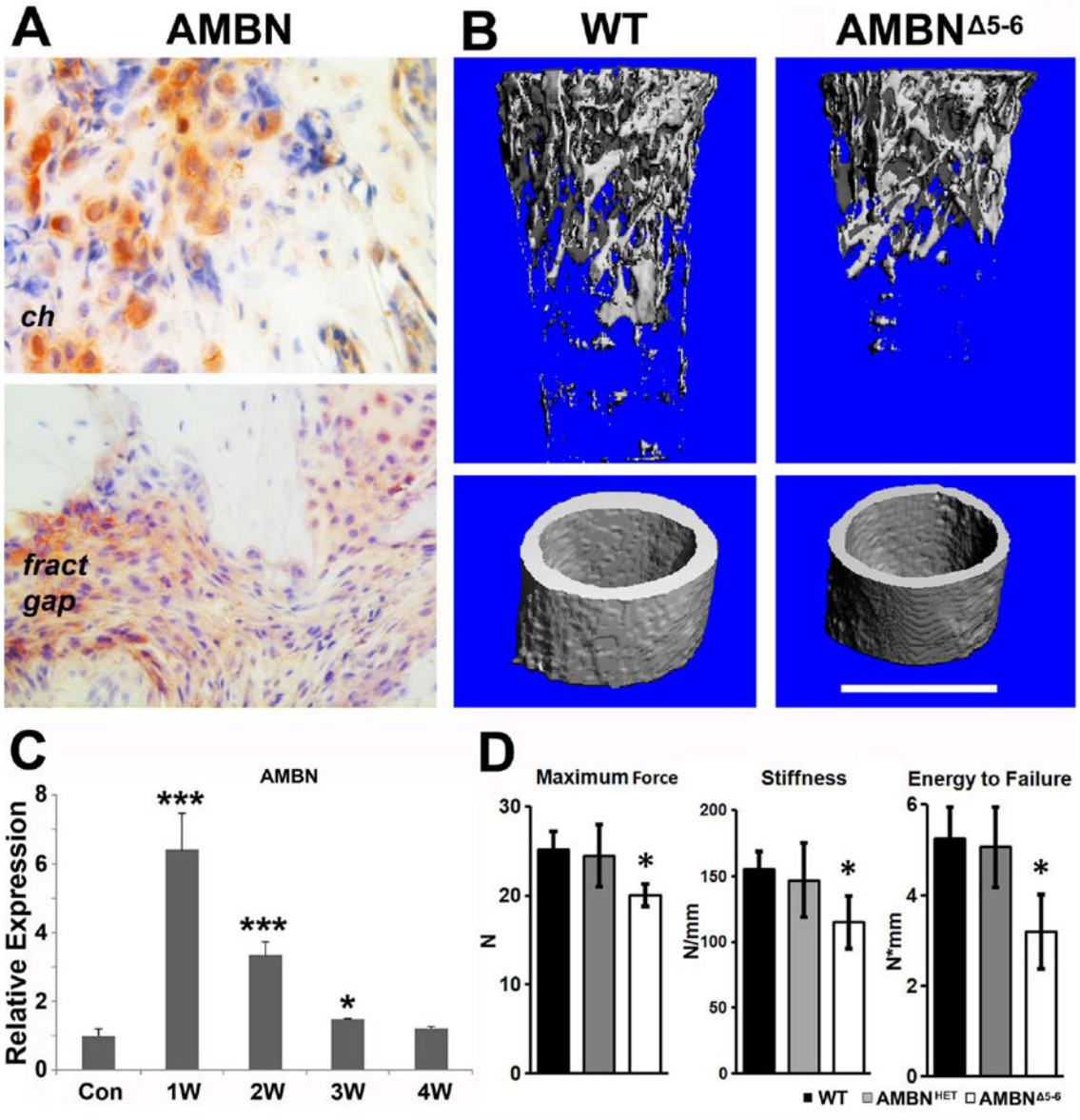

Figure 1. Differences in bone structure and mechanical properties in AMBN mutant mice versus controls

(A) Immunohistochemical analysis of AMBN protein expression and localization in periosteal callus of WT mouse fractured tibia. (B) 3D reconstruction of μ-CT images from WT and AMBN$^{\Delta 5\text{-}6}$ femurs of 3 month old mice. Bar= 1mm. (C) qRT-PCR analysis of Ambn gene expression during tibia fracture healing. (D) Maximum Force, stiffness, and energy to failure measurements generated by femur 3-point bending tests. Data are presented as mean ± SD. * $p < 0.05$.

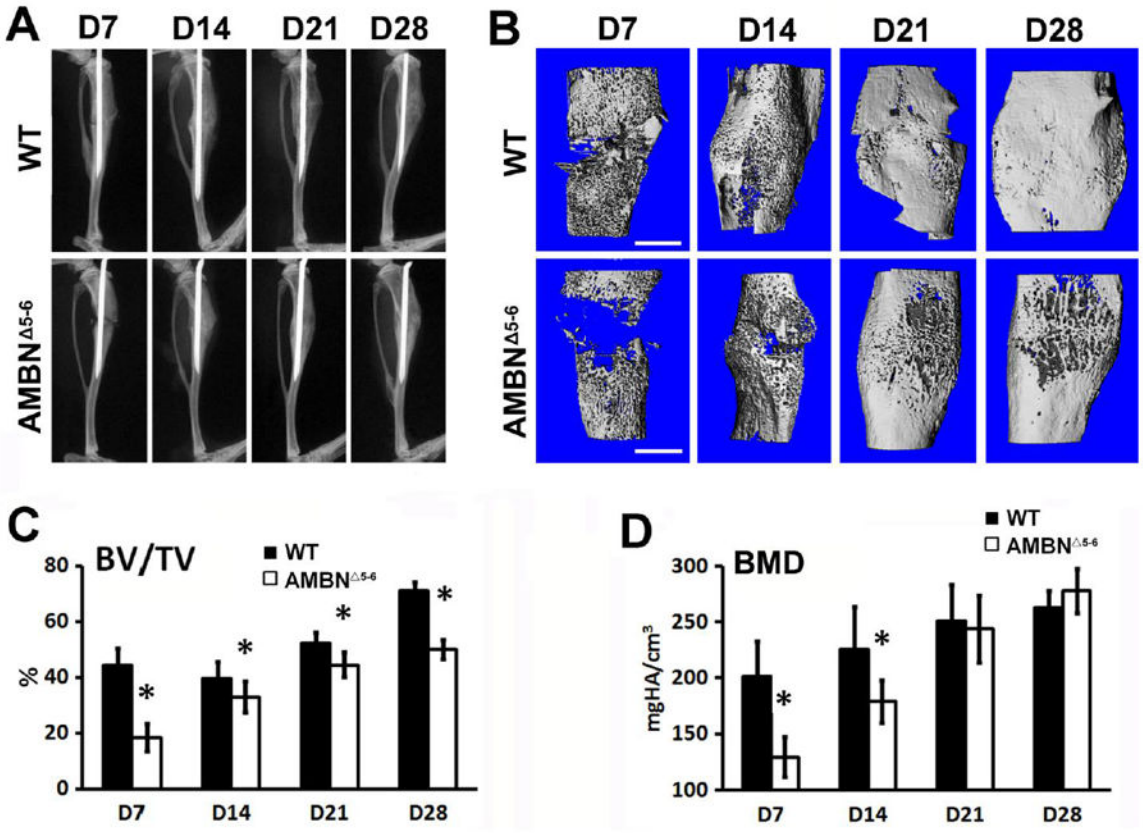

Figure 2. Delayed bone fracture healing in AMBN$^{\Delta 5\text{-}6}$ mice

(A) X-ray radiographic comparison of the fracture sites 7, 14, 21, and 28 days post-surgery between WT and AMBN mutant mice. (B) 3D reconstruction of μ-CT images of the fracture callus illustrating the morphology and mineralized state of the callus tissue on post-operative days 7, 14, 21, and 28. Bar=1mm. (C, D) Callus bone volume (BV/TV) (C) and bone mineral density (BMD) (D) in WT and AMBN mutant mice. Data are presented as mean ± SD. * $p < 0.05$

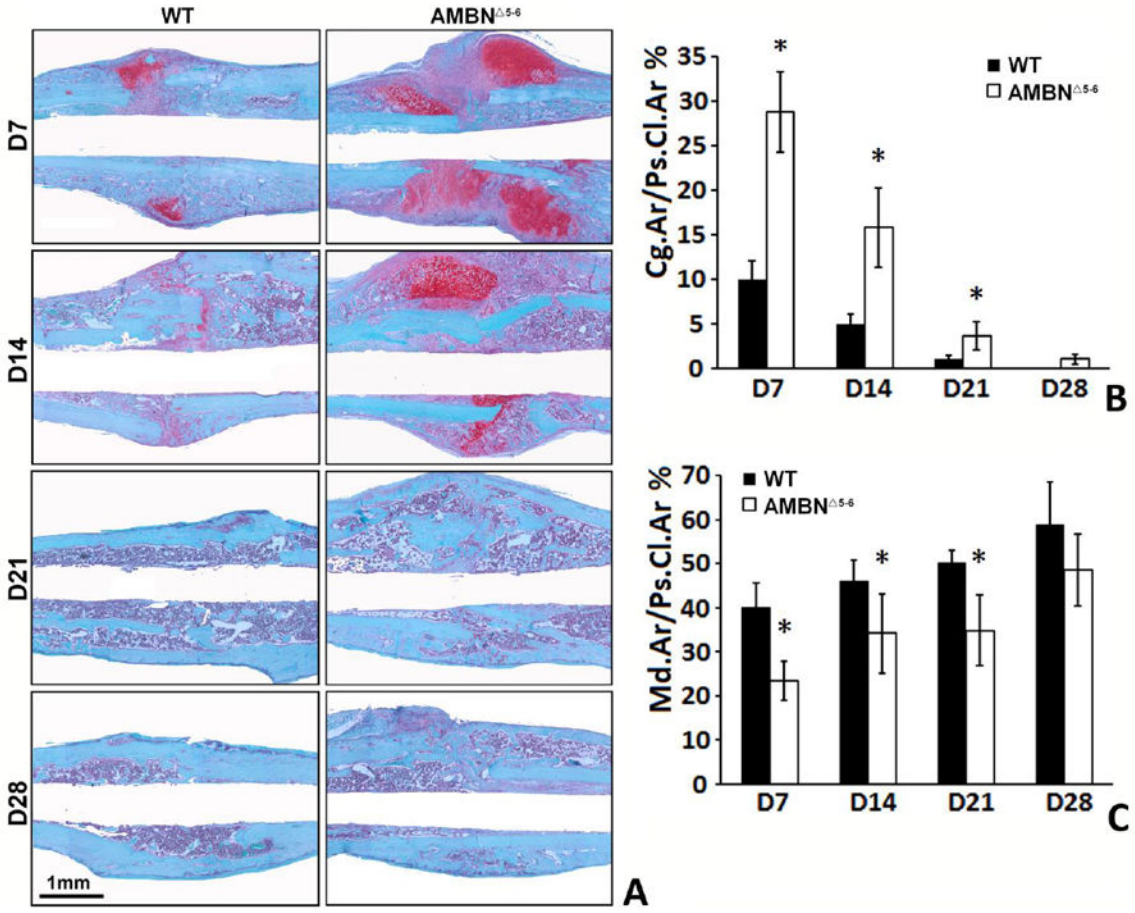

Figure 3. Histological analysis of AMBN$^{\Delta 5\text{-}6}$ and WT mice during fracture healing

(A)The sections were stained with Safranin O/fast green to mark cartilage (red) and mineralized tissue (green) of AMBN$^{\Delta 5\text{-}6}$ and WT mice on post-operative days 7, 14, 21, and 28. Bar = 1mm. (B, C) Histomorphometric quantification of cartilage area versus periosteal callus area (Cg.Ar./Ps.Cl.Ar.%) (B) and mineralized area versus periosteal callus area (Md.Ar./Ps.Cl.Ar.%) (C) between WT and AMBN mutant group during the fracture healing stage. Data are presented as mean ± SD. * $p < 0.05$

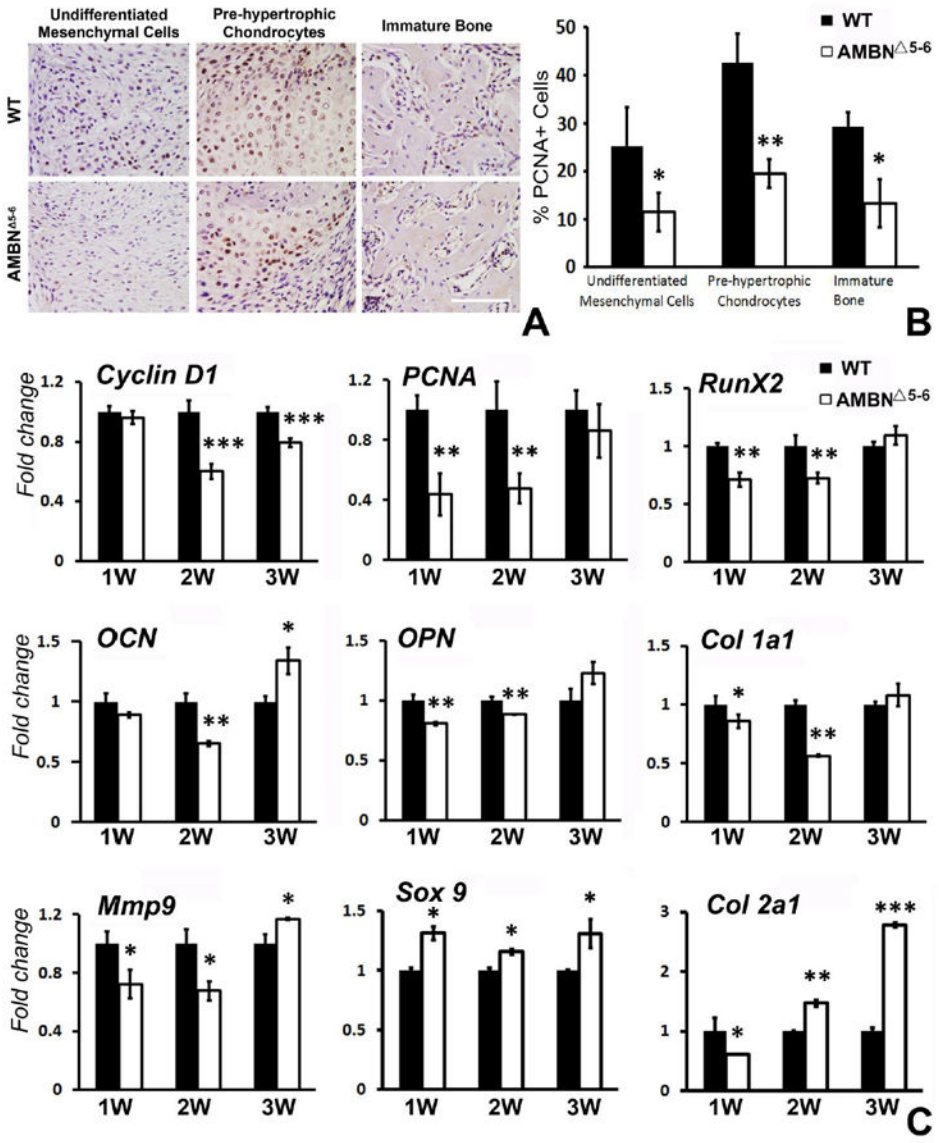

Figure 4. Differences in gene expression and cell proliferation between WT and AMBN$^{\Delta 5\text{-}6}$ mice

(A) PCNA immunostaining in the areas of undifferentiated mesenchymal, pre-hypertrophic chondrocytes and immature bone. Images were acquired at 400× magnification. (B) Percentile of PCNA positive cells in undifferentiated mesenchymal, pre-hypertrophic chondrocytes and immature bone. (C) RT-Real time qPCR analysis of cell proliferation-related markers PCNA and Cyclin D1, bone markers Runx2, OCN, OPN, and Col 1a1, and cartilage markers Sox9 and Col 2a1, and the extracellular matrix degrading metalloproteinase MMP9. The relative expression levels are presented as mean ± SD. * $p < 0.05$, ** $p < 0.01$, *** $p < 0.001$.

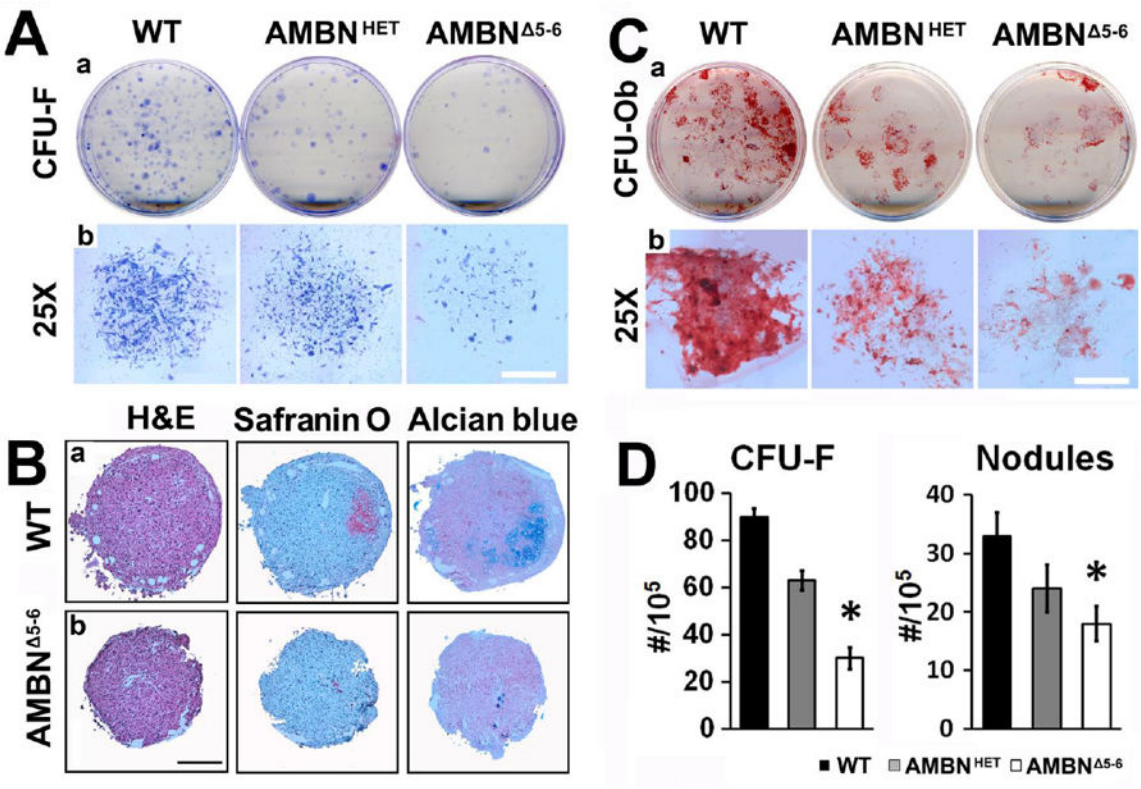

Figure 5. Proliferation and differentiation potential of BMSCs from WT and AMBN mutant mice

(A, C) Representative colony forming units (CFU) assays from WT and AMBN mutant BMSCs. The CFU-F assays (A) were conducted by culturing BMSCs for 14 days and then stained with Giemsa. The CFU-Ob assays (C) were performed by culturing BMSCs in growth medium for 14 days followed by osteogenic medium for 7 days, and mineral nodules were visualized by Alizarin red staining. (B) H&E, Safranin O and Alcian blue staining of cultured aggregates. (D) The number of CFU-F and CFU-Ob colonies were counted after 14 (CFU-F) and 21 (CFU-Ob) days culture. Data were obtained based on duplicates from 4 different animals in each genotype group, and values are presented as mean ± SD. * = $p<0.05$.

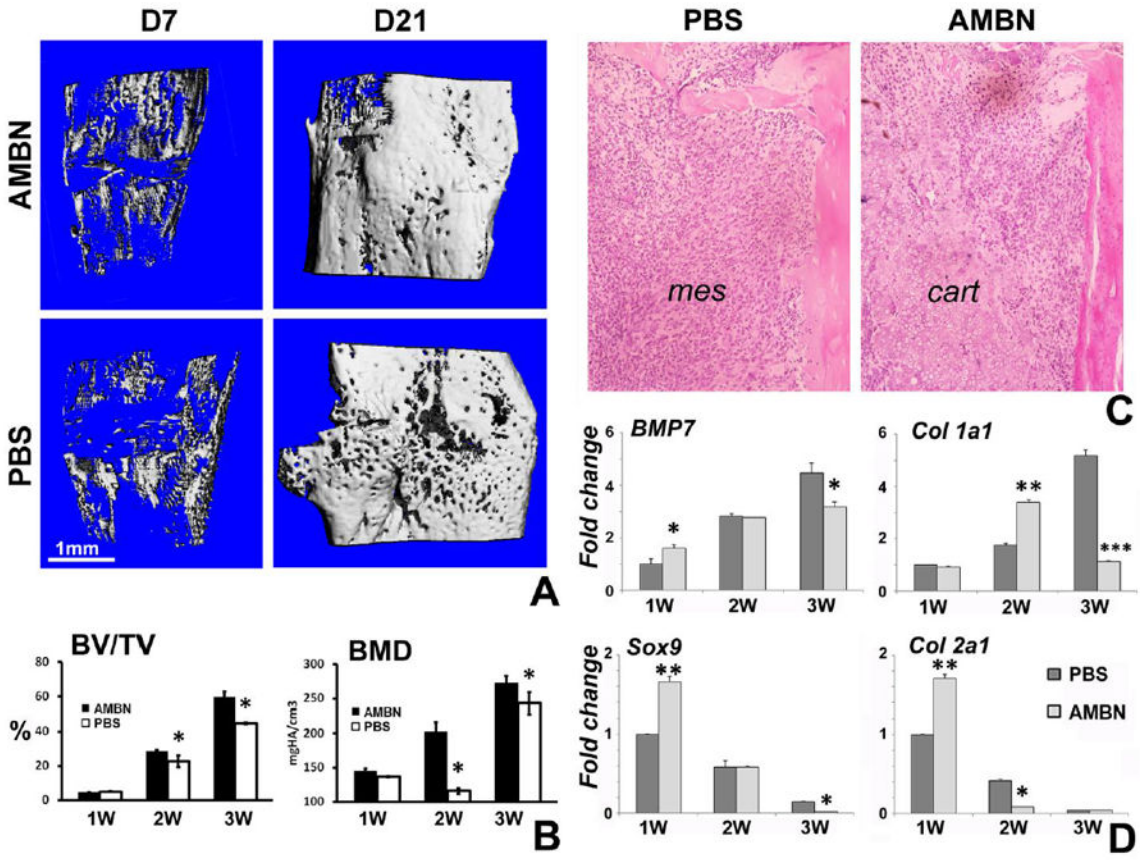

Figure 6. Accelerated fracture healing after application of exogenous AMBN protein

(A) 3D μ-CT images of tibia fracture zones in AMBN treated (AMBN) and untreated controls (PBS) 7 days and 21 days post-surgery. Bar=1 mm. (B) Callus bone volume (BV/TV) (C) and bone mineral density (BMD). (C) H&E staining of tibia fracture zones from PBS- and AMBN-treated groups on D7 post-surgery. The fracture gap was filled with mesenchymal cells (mes) in the control (PBS) and cartilage tissue (cart) in the AMBN treated group. (D) RT-Real time qPCR analysis of relative gene expression of bone (BMP7, Collagen I) and cartilage (Sox9, Collagen II) marker genes in WT and AMBN mutant mice. (D). Data are presented as mean ± SD. * $p<0.05$, ** $p<0.01$.

TABLE I

PCR Primer Sequences

Genes	Sequences	Genes	Sequences
AMBN	F1 5′CAAGTTGCCTTACCCCAAGA3′ R1 5′TTGGGGTTATTGGAGTGGAG3′ R2 5′AAGCGAAGGAGCAAAGCTGCTATT3′	Col 1a	F 5’TGGCAAGAATGGAGATGATG R 5’ACCATCCAAACCACTGAAGC
Cyclin D1	F 5’GCGTACCCTGACACCAATCT R 5’ATCTCCTTCTGCACGCACTT	MMP9	F 5’AGTTGCCCCTACTGGAAGGT R 5’GTGGATAGCTCGGTGGTGTT
PCNA	F 5’GGTTGGTAGTTGTCGCTGT R 5’CGGAGTTGTGGCGACTAGAT	SOX 9	F 5’CAAGACTCTGGGCAAGCTC R 5’GGGCTGGTACTTGTAATCGG
Runx2	F 5’TCTGGCCTTCCTCTCTCAG R 5’GGATGAAATGCTTGGGAAC	Col 2a	F 5’TGGCTTCCACTTCAGCTATG R 5’AGGTAGGCGATGCTGTTCTT
OCN	F 5’GCGCTCTGTCTCTCTGACCT R 5’ACCTTATTGCCCTCCTGCTT	BMP7	F 5’ACTACATCCGGGAGCGATTTGACA R 5’TATCAAACACCAACCAGCCCTCCT
OPN	F 5’TCTGATGAGACCGTCACTGC R 5’CCTCAGTCCATAAGCCAAGC	β-Actin	F 5’AAATCGTGCGTGACATCAAA R 5’TCTCCAGGGAGGAAGAGGAT

TABLE II

FEMUR BIOMECHANICAL PROPERTIES IN 3-MONTH-OLD MALE MICE

	WT	AMBN^{HET}	AMBN$^{\Delta 5\text{-}6}$
Total Area(mm^2)	1.70±0.19	1.67±0.19	1.58±0.13
Stiffness (N/mm)	155.41±13.11	147.03±27.91	135.13±20.00 *
Maximum force(N)	25.10±4.08	24.49±4.48	21.06±1.28 *
Maximum stress(Mpa)	14.27±3.01	14.05±2.13	13.42±1.81
Energy to failure(N*mm)	5.25±2.65	5.06±0.88	3.2±1.22 *

Data are presented as means ± SD from 5 to 6 individual mice.

* = P<0.05 AMBN$^{\Delta 5\text{-}6}$ mutant mice versus wild-type control.